Construction and Building Materials 385 (2023) 131516

Contents lists available at ScienceDirect

Construction and Building Materials

journal homepage: www.elsevier.com/locate/conbuildmat

Prediction of compressive strengths of pumice-and diatomite-containing cement mortars with artificial intelligence-based applications

Burak Kocak [a], İbrahim Pınarcı [b], Uğur Güvenç [c], Yilmaz Kocak [d,*]

[a] Duzce University, Graduate School of Education, Department of Electrical Electronics Engineering, Turkey
[b] Bilecik Seyh Edebali University, Pazaryeri Vocational School, Department of Design, Turkey
[c] Duzce University, Faculty of Engineering, Department of Electrical-Electronics Engineering, Turkey
[d] Duzce University, Faculty of Engineering, Department of Civil Engineering, Turkey

ARTICLE INFO

Keywords:
Pumice
Diatomite
Compressive strength
ANN
ANFIS

ABSTRACT

In this study, two different Artificial neural networks (ANN) and two different adaptive network-based fuzzy inference systems (ANFIS) models were constructed to predict the compressive strength of 7 different cement mortar samples with or without pumice and/or diatomite on different days. Five parameters including day, PC, pumice, diatomite and water were employed as the inputs, and the compressive strength was used as the output variable. The compressive strengths used in the model construction were obtained from laboratory experiments accounting for a total of 168 data. Statistical methods such as R^2, RMS and MAPE preferred in the literature were used to compare the four different models. According to the test results obtained from R^2, RMS and MAPE, ANN and ANFIS models were able to make very good predictions performance. For this reason, it can be said that these cement mortars' compressive strength can be estimated with a very small error and in a short time with both ANN and ANFIS models.

1. Introduction

The harmful effects of cement industries on the environment are well-known fact. Recent studies have shown that Portland Cement (PC) production in the cement industries consumes 5% of the industrial energy and causes 7% release of CO_2 emissions worldwide. It is stated that the emission CO_2 causes approximately 65% of global warming [1,2]. Therefore, to reduce CO_2 emissions and the high carbon footprint originating from the construction industry, there is required to reduce cement production amount. To reduce the amount of cement production, alternative environmentally friendly binding materials should be used in the construction industries [3]. These materials such as zeolite [4], pumice [5], diatomite [6], fly ash [7], silica fume [8], blast furnace slag [9], rice husk ash [10], locally available in many countries, have been widely used as supplementary cementitious material (SCM) in many research in cement and concrete technology. The main advantage of SCMs is that they decrease the CO_2 emissions released into the atmosphere during cement production by reducing the amount of cement by 5–30% [11,12]. Also, SCMs are pozzolanic materials. Moreover, substituted SCMs into cement or concrete, the mechanical strength and durability of concrete are increased [13–16]. Therefore, using SCMs is a good choice to reduce the amount of cement in concrete and enhance concrete strength and durability.

In this context, pumice and diatomite are used intensively in the construction sector due to the improvement effect of cement mortar and concrete properties. The mechanical properties of concrete and cement mortar do not exhibit a strong linear structure as they are derived from the different parameters involved in their composition. For this reason, it can be said that a tool that can help quantitatively in the optimum design of cement-based mortars and concretes has not yet been determined, despite a lot of research on these materials. Therefore, it has been tried to develop analytical formulas for the estimation of the mechanical properties of cement mortars and concretes by using deterministic methods. In these studies, it is emphasized that approaches such as artificial intelligence, machine learning, multiple nonlinear regression and multiple linear regression have been successfully applied [17–23].

Artificial neural networks (ANN) and adaptive network-based fuzzy inference systems (ANFIS) have been developed as popular artificial intelligence modeling techniques that can solve many engineering problems in recent years. Since these models can be created using a limited number of data sets during the training phase and their ability to predict responses in complex systems, they have been successfully used

* Corresponding author at: Duzce University, Faculty of Engineering, Department of Civil Engineering, Konuralp Campus, Duzce, Turkey.
E-mail address: yilmazkocak@duzce.edu.tr (Y. Kocak).

https://doi.org/10.1016/j.conbuildmat.2023.131516
Received 9 January 2023; Received in revised form 17 April 2023; Accepted 19 April 2023
Available online 27 April 2023

in many studies to predict the mechanical properties of concrete and cement mortar. Chithra et al. (2016) created models with ANN and multiple regression analysis (MRA) to predict the compressive strength of high-performance concrete of cement mortars containing copper slag and nano silica. In their laboratory studies, they used cement mortars containing 0, 10, 20, 30, 40 and 50% ratios of copper slag as partial fine aggregate replacement as well as containing 0, 0.5, 1, 1.5, 2, 2.5 and 3% ratios of nano silica as partial cement replacement. 264 samples were prepared with these mortars, and their compressive strengths were determined at age of 1, 3, 7, 28, 56 and 90-days. Using the data obtained, different ANN models were created and the data obtained from these models were compared with the data obtained by MRA. As a result, it was stated that the results obtained from the ANN model were closer to the real results and had a higher correlation [24]. Behnood et al. (2015), on the other hand, developed models using ANN, non-linear regression (NLR) analysis, M5′ model tree (MT) and support vector machine (SVM) techniques to estimate the tensile strength of steel fiber-reinforced and unreinforced concretes. They used error measures to compare the performance of the developed models and the different models developed by other researchers. They used error measures to compare the performances of their developed models and the different models developed by other researchers. As a result, they stated that ANN provides superior results compared to other model analyses [25]. In another study, Kocak and Gulbandilar (2016) tried to estimate the compressive strengths of 63 samples of 7 concrete types produced with zeolite and diatomite, which they were exposed to the effect of $MgSO_4$, at age of 2, 56 and 90-days with ANFIS. In the study, the results obtained from the models and the experimental results were statistically compared. According to these results; They pointed out that the experimental results and the prediction results are very close to each other and that the model created with ANFIS is powerful and useful [26]. Armaghani and Asteris (2021) tried to estimate the mortars' compressive strength produced with metakaolin substituted cement with ANN and ANFIS in their study. For this, they compared the ANN and ANFIS models, which they created using the experimental results they obtained from the literature. They used metakaolin/binder ratio, hydration age, water/binder ratio, maximum aggregate diameter, binder/sand ratio, and superplasticizer values as inputs, compressive strength values as output in the models. To determine performances of the values they obtained, they compared the best ANFIS and the best ANN model by using statistical methods such as RMSE, R^2, a10 index, VAF and MAE. They stated that both ANFIS and ANN models gave very good results according to the data determined by statistical methods, but the results obtained with ANN were closer to the real results [27]. In another study, Amin et al. (2021) tried to estimate the mortars' compressive strength produced with natural volcanic ash by creating models with ANN and ANFIS techniques. They used around 150 data from the literature for training and testing the models. They also produced mortar samples containing different ratios of volcanic ash, and determined the compressive strength of these samples. They used this data to confirm the results obtained from the models. According to the results obtained, they stated that the R^2 values of the models created with both ANN and ANFIS were above 0.9, and therefore the compressive strength values could be estimated well and accurately [3].

The cement mortar samples' compressive strength can be expressed as one of the most important parameters among the determining factors in cement production. Due to the cost and time-consuming nature of performing compressive strength tests, many researchers are trying to develop models to predict compressive strength simply and accurately with artificial intelligence-based applications. For this reason, there are many studies in the literature describing the compressive strength estimation of various cementitious composites. However, it is known that the compressive strength results differ according to the properties of the cement and supplementary cementitious material used. For this reason, it is thought that different physicochemical properties of cement, pumice and diatomite used in the study will contribute to the literature. For this purpose, the compressive strengths of cement-based mortar samples with or without pumice and diatomite have been examined developing two different ANN and two different ANFIS techniques in this study. Compressive strength results of 168 cement mortar samples have been used to improve ANN and ANFIS models. Based on this database, five parameters including age of samples (days), PC, pumice, diatomite and water, were used as input parameters, while the value of compressive strengths was used as output parameter. According to the obtained data, it has been concluded that the developed ANN and ANFIS models exhibit high reliability and very successful.

2. Experimental study

In the preparation of mortar samples, PC, pumice, diatomite, standard sand and water were used. PC is CEM I 42.5 R type cement produced at the Eskisehir ÇİMSA Plant (Turkey) compliant with TS EN 197-1 standard [28]. [17]. Pumice and diatomite used as supplementary cementitious materials in the preparation of the mortar samples were provided from Isparta Betas and EP mineral commercial companies, respectively. The pumice has been grounded in a ball mill for 30 min.

Microstructure analyses of PC, diatomite and pumice were determined with an FEI Quanta FEG 250 model device. The XRD patterns of the materials were conducted with Rikagu SmartLab XRD device using Cu Kα (λ = 1.54 A°) radiation with the 2θ range of 5° to 70°. FT–IR analyses were determined with Shimadzu IRPrestige 21 device.Chemical analyses of PC, pumice and diatomite were performed by ARL 9900 Intellipower X-ray Analyzer. Specific gravity by Quanta Chrome MVP–1, Blaine by Toni Technik 7202, and fineness determination by Hosokawa 200 LSN (air jet sieve) were performed.

The images of PC, pumice and diatomite are shown in Fig. 1a, 1b and 1c, respectively.

As can be seen from Fig. 1(a, b and c), PC, pumice and diatomite contain porous structures. Moreover, while pumice has an irregular plate shape and irregular morphology, diatomite has micropores structures of different sizes and shapes (Fig. 1-b and c). As seen from Fig. 1c, the micropores of diatomite are usually connected, and intergranular micropores have non–uniform shapes as their walls are composed of haphazard spaced diatom frustules, detrited quartz and non–uniform deposits of other mineral substances [29–31].

The XRD patterns of PC, pumice and diatomite are shown in Fig. 2.

According to XRD pattern of PC, the main components are $3CaOSiO_3$ (C_3S), $2CaOSiO_3$ (C_2S), 4CaO. Al_2O_3 $3Fe_2O_3$ (C_4AF) and $3CaO.Al_2O_3$ (C_3A), (Fig. 2-a). Pumice has an amorphous structure consisted amorphous quartz (SiO_2) material at 2θ = 20–32°. And also, it has some crystalline phases as calcite ($CaCO_3$), anorthite ($CaAl_2Si_2O_8$) and albite ($NaAlSi_3O_8$) [29,32] (Fig. 2-b). The wide reflection in the range of 2θ = 15–38° seen in diatomite shows that it also has an amorphous structure. Furthermore, peaks at 2θ = 34.86°, 27.61° and 21.76° are related to quartz (Fig. 2-c) [31,33].

The FT-IR patterns of PC, pumice and diatomite are shown in Fig. 3.

In FT–IR spectrum of PC, the strong band at 507 cm^{-1} related to the Al–O bond appearing along with Si–O was observed. The peak at 902 cm^{-1} is attributed to Si–O bond in cage structures. The peaks at 735 and 1124 cm^{-1} are related to the existence of S–O bonds, displaying the plaster in PC. Band at 1413 cm^{-1} is represented the CO_3^{-2} (Fig. 3-a) [34–36]. As detected from the spectrum of pumice, the small band at 1424 cm^{-1} is assigned by CH bonds. Strong peak at 997 cm^{-1} is associated with symmetric stretching vibration of Si–O–(Si, Al) bonds. Weaker peak at 708 cm^{-1} can be allocated with Si–O bending strength vibrations of amorphous quartz. The peaks at 542 and 435 cm^{-1} can be attributed to Al–O bond appearing along with Si–O (Fig. 3-b) [29,37,38]. The peaks at 3388 cm^{-1} and 1633 cm^{-1} seen in Fig. 3-c are associated with the O–H group of water in diatomite. The strong peak at 1066 cm^{-1} indicates the stretching vibration of Si–O–Si group. The peak at 798 cm^{-1} are related the vibration of SiO–H group. The peaks at 448 and 551 cm^{-1} represent the bending vibration of Si–O (Fig. 3-c). These

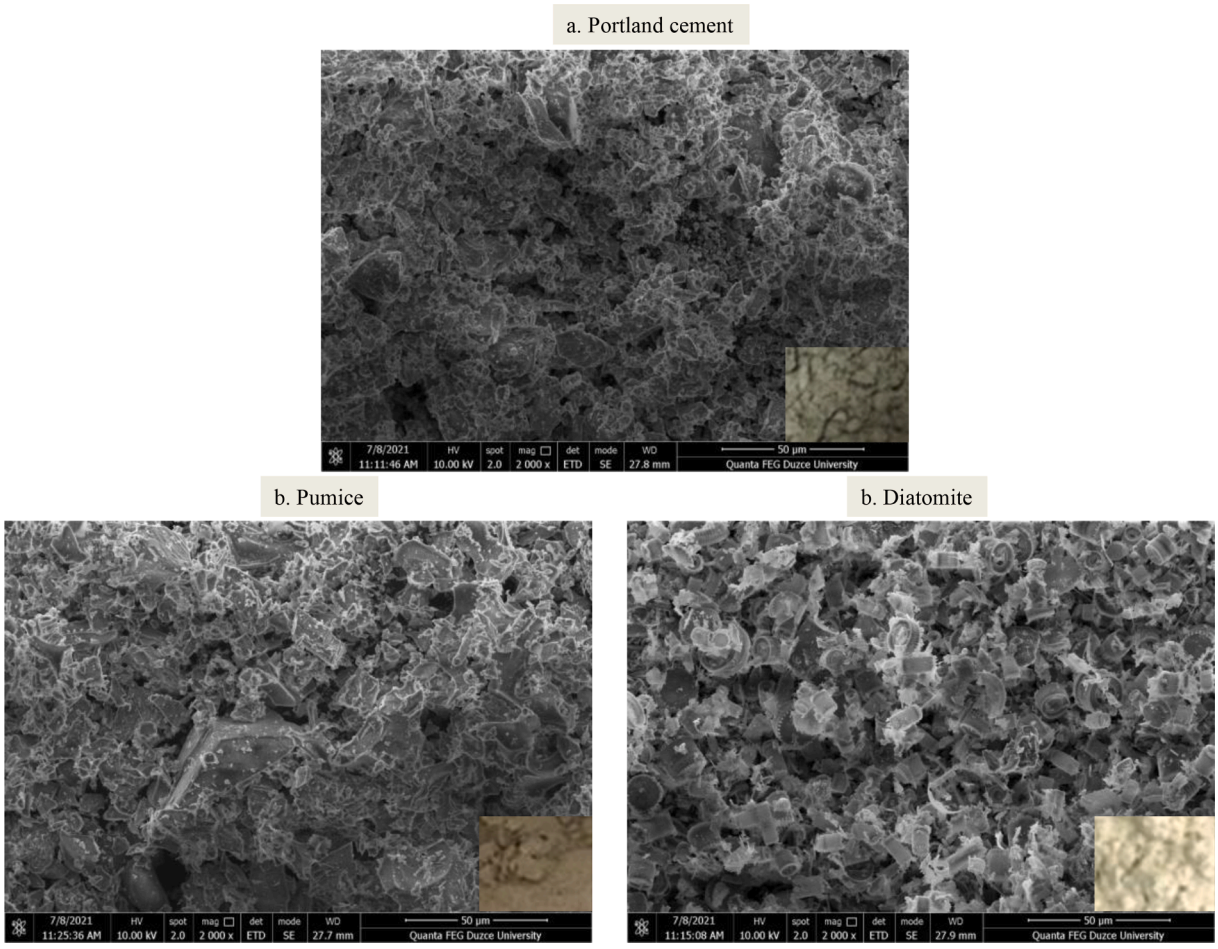

Fig. 1. The images of PC, pumice and diatomite viewed by electron microscope.

characteristic peaks indicate that diatomite is mainly composed of SiO_2 [30,39,40].

Chemical and physical specifications of the PC, pumice and diatomite are given in Tables 1 and 2, respectively.

By the chemical compositions of PC, the chief components are CaO and SiO_2, respectively. Furthermore, the PC contains Al_2O_3, SO_3, Fe_2O_3, MgO, and traces of K_2O, Na_2O, respectively. The chief components of pumice are SiO_2 and Al_2O_3, respectively. Additionally, the pumice contains K_2O, Na_2O, CaO, Fe_2O_3, and MgO and traces of SO_3. The chief components of diatomite are SiO_2. The high silica content indicates that diatomite has pozzolanic activity. Also, the diatomite contains Al_2O_3 and traces of Fe_2O_3, CaO, MgO, Na_2O, K_2O and SO_3 (Table 1). Furthermore, the mass fractions of S + A + F for pumice and diatomite are 76.76% and 88.75, respectively. This shows that pumice and diatomite comply with the specified conditions (S + A + F > 70%) to be defined as natural pozzolan [41].

The Blaine of PC, pumice and diatomite are 3822, 2645 and 6112 cm^2/g, respectively. The specific weight of PC, pumice and diatomite are 3.18, 2.70 and 3.18 g/cm^3, respectively. The residue on the 45 μm sieve of PC, pumice and diatomite are 3.2%, 40.5%, and 0.1%, respectively. Also, the residue on 90 μm sieve of PC, pumice and diatomite are 0%, 7.8%, and 0%, respectively (Table 2).

In the study, a total of seven different cement were used. These types of cement have been produced by substituting pumice and/or diatomite at the ratios of 0%, 5%, 10%, 5 + 5%, and 10 + 10%. The properties and codes of the mortar mixtures prepared with these types of cement are given in Table 3.

The cement mortar samples, which prepared according to the mixture amounts in Table 3, were poured into three gang prism molds of size 40x40x160 mm, and then each mold was placed in the jolting apparatus and jolting according to the principles in TS EN 196-1 [42]. These mortar samples obtained were kept in the laboratory for 24 h. After 24 h, these samples were taken out of the molds and placed in the curing pool at a temperature of 20.0 ± 1.0 °C. These samples were removed from the curing pool at age of 2, 7, 28 and 90-days, dried with the help of a cloth and properly broken from halves of the prism. A total of 168 compressive strength results obtained from six half-prism mortar samples for each cement and hydration day were determined under the principles in the TS EN 196-1 standard [42].

3. Artificial neural network

ANN is one of the most generally used statistical models configured from simulating organizational principles of the nervous system functions [27,43]. ANN is developed by getting inspired by the real nervous system and consists of series of interconnected neurons which are arranged in layers like the human brain [43,44]. ANN determines the relationship between input–output through a series of data structures connected with a few neurons [43]. The ANN structure can either be feed-forward or back-propagation neural network, and, every type of ANN has its advantages and disadvantages for different data sets [3,43]. Feedforward neural networks utilize one-way link to establish relation between input parameters and target values, and neurons in different layers are also bonded with one-way setups [3]. Back propagation neural network occurs of three main layers which are input layer, one or a few hidden layers, and output layer. In these networks, signals are obtained at the input layer and transferred to the first hidden layer for processing. The values from every input neuron are then multiplied by

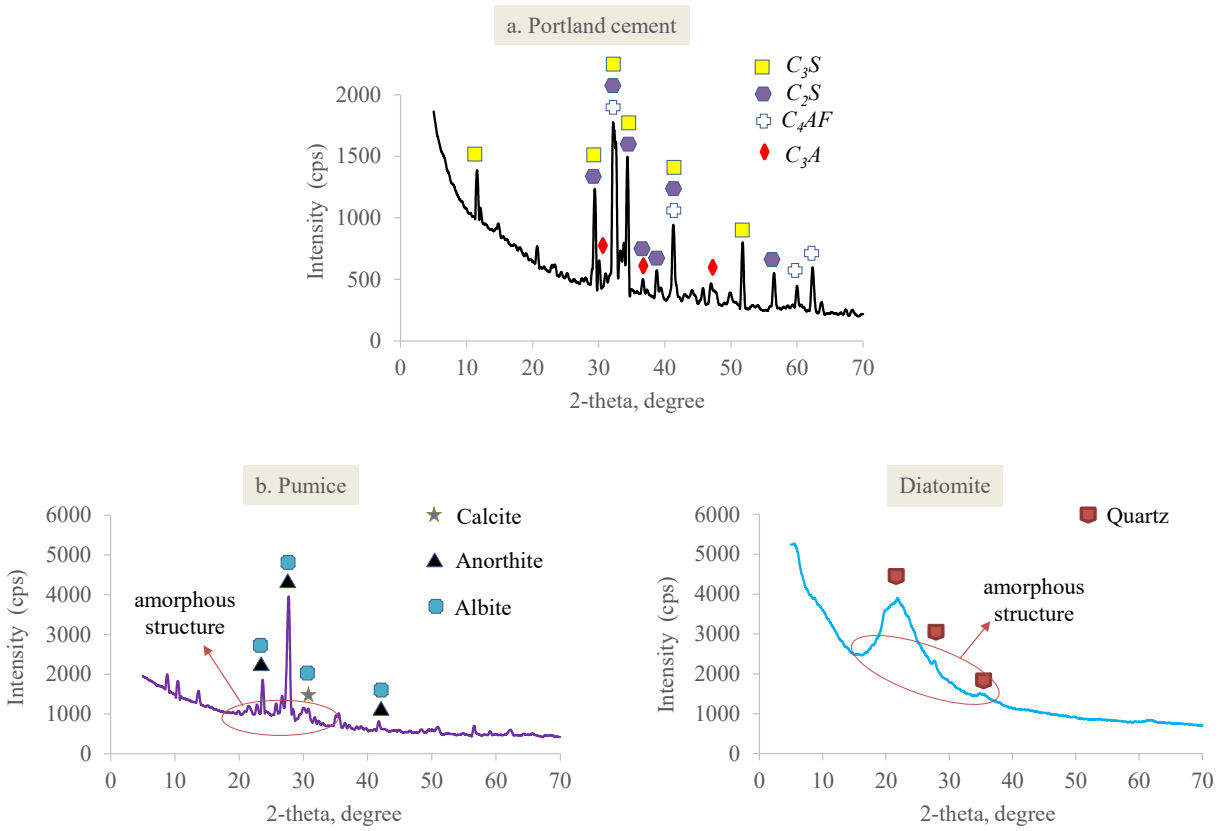

Fig. 2. The XRD patterns of PC, pumice and diatomite.

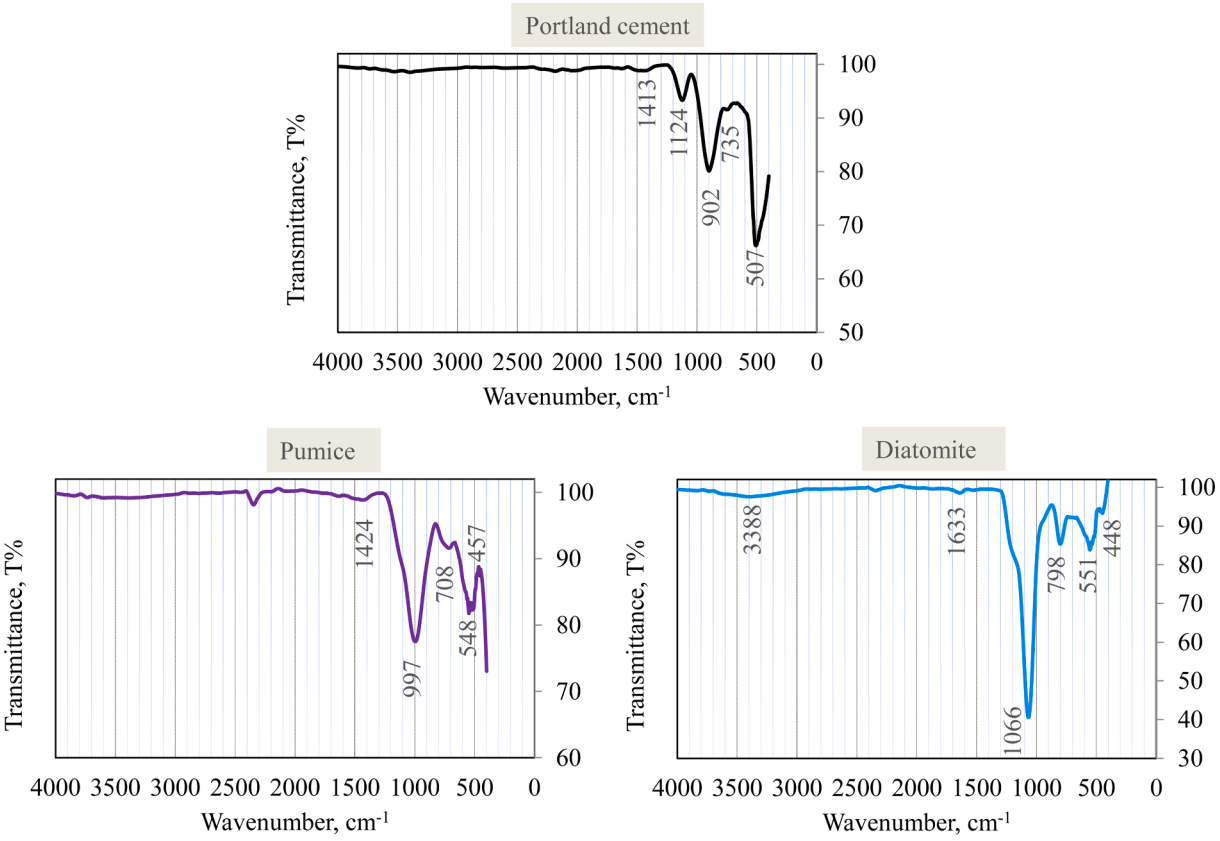

Fig. 3. FT-IR patterns of PC, pumice and diatomite.

Table 1
Chemical compositions of PC, pumice and diatomite.

Materials	Chemical composition, (% of oxides by weight)										
	SiO_2 (S)	Al_2O_3 (A)	Fe_2O_3 (F)	CaO	MgO	SO_3	Na_2O	K_2O	Cl^-	LOI	Free CaO
PC	20.36	4.6	2.56	62.57	1.53	3.32	0.26	0.66	0.018	2.38	1.78
Pumice	56.32	16.51	3.93	4.84	1.87	0.23	5.18	5.09	0.01	2.65	–
Diatomite	85.69	2.1	0.96	0.54	0.32	0.03	0.25	0.18	0.013	9.97	–

Table 2
Physical specifications of PC, pumice and diatomite.

Materials	Specific gravity, g/cm^3	Blaine, cm^2/g	Range dimension (over sieve), %	
			>45 μm	>90 μm
PC	3.18	3822	3.2	0.0
Pumice	2.70	2645	40.5	7.8
Diatomite	2.58	6112	0.1	0.0

Table 3
Properties and codes of the mortar mixtures.

Cement codes	PC, g	Pumice, g	Diatomite, g	Water, g	Standard sand, g	w/b
R	450	0	0	225	1350	0.5
P10	405	45	45	225		0.5
P20	360	90	90	225		0.5
D10	405	0	0	250		0.55
D20	360	0	0	270		0.6
P5D5	405	22.5	22.5	240		0.53
P10D10	360	45	45	250		0.55

every of the connection weights which are linking the input layer neurons to hidden layer neurons [45]. Then, the input values for each neuron of the hidden layer are summed, and a bias value is added [43,46]. The calculated weighted sum is then passed through the activation function and presented to the output layer. Based on the feedforward and the back-propagation (Fig. 4), the outputs can be calculated as a sigmoid of logistic transfer function using Eq. (1) [21,25].

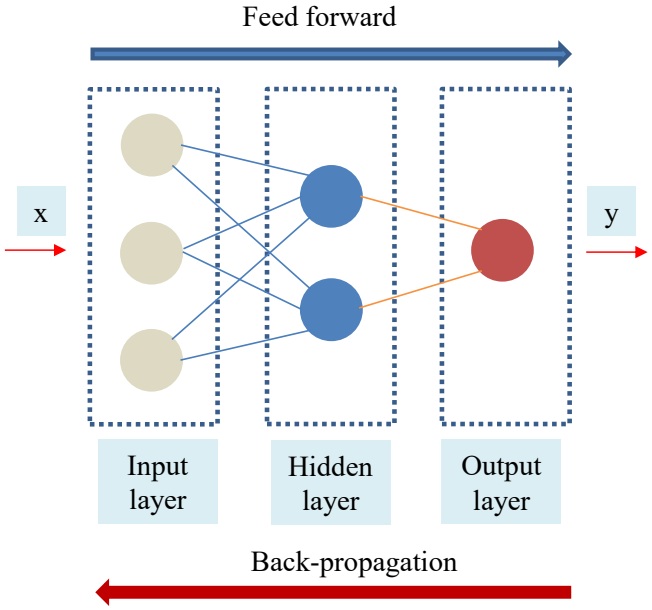

Fig. 4. Structure of backpropagation neural networks model [21].

$$y_j = f(net) = \frac{1}{1 + e^{-\sum w_{ij} x_i + b}} \quad (1)$$

In Eq. (1), y_j is the output signal, and f is the activation function in the terms of the calculated network value (net). w_{ij} is the connection weight between neurons i and j in the lower and upper layers, respectively. x_i and b are the output of neuron i and bias value of the network, respectively [25,46].

Among the ANN methods, backpropagation algorithms have been commonly used to train neural network. Thus, feedforward backpropagation neural network and Elman backpropagation neural network have been used as the backpropagation algorithms in the study.

4. Adaptive network-based fuzzy inference system

ANFIS is a neural network based on the Takagi-Sugeno fuzzy system that simulates human reasoning when dealing with complex nonlinear problems where other classical approaches fail. ANFIS can take advantage of both features in a single format by combining two separate techniques as neural networks and fuzzy logic. In ANFIS, the reasoning steps are performed with a fuzzy inference system, and the information between the input and output variables of an engineering system are defined as IF – THEN fuzzy rules [47–49]. Basic architecture of an ANFIS algorithm for two input variables × and y depicts in Fig. 5.

The two IF-THEN rules stated in Eqs. (2) and (3) are indicated [47,50].

$$Rule\ 1\text{- }IF\ x\ is\ A_1,\ and\ y\ is\ B_1\ THEN\ f_1 = p_1\ x + q_1\ y + r_1 \quad (2)$$

$$Rule\ 2\text{- }IF\ x\ is\ A_2,\ and\ y\ is\ B_2\ THEN\ f_2 = p_2\ x + q_2\ y + r_2 \quad (3)$$

In Rules 1 and 2, A_i and B_i represent the membership functions for inputs × and *y*, respectively, f_1 and f_2 are the output function, and p_i, q_i, and r_i are the consequent parameters.

The expressions of these layers in the Fig. 5 can be stated as stated below [3,47–51]:

Layer 1: In this layer named fuzzification layer, the output of every point is the membership degree value, which gives by the inputs of the membership functions. In this layer, the required values such as membership functions in Eqs. (4) and (5) are shown.

$$o_{l,1} = \mu A_{(i)}(x), for\ i = 1, 2, \quad (4)$$

$$o_{l,1} = \mu B_{(i-2)}(y), for\ i = 3, 4 \quad (5)$$

In Eqs. (4) and (5), *i* is the number of input variables, $\mu A_{(i)}$ *and* $\mu B_{(i-2)}$ *are* the membership functions for fuzzy set A_i or $B_{i\text{-}2}$, *respectively*. $o_{l,1}$ is shown in Eq. (6).

$$o_{l,1} = \mu A_i(x) = \frac{1}{1 + \left[(x - c_i)/a_i\right]^{2b_i}} \quad (6)$$

In Eq. (6), a_i, b_i and c_i are the variables that influence membership functions.

Layer 2: Each node in this layer, which is called the rule layer, is determined by the fuzzy extraction of a rule and the algebraic multiplication operator. $o_{l,2}$ is shown in Eq. (7).

$$o_{l,2} = w_i = \mu A_i(x).\mu B_i(y) \text{ için } i = 1, 2, \cdots, n \quad (7)$$

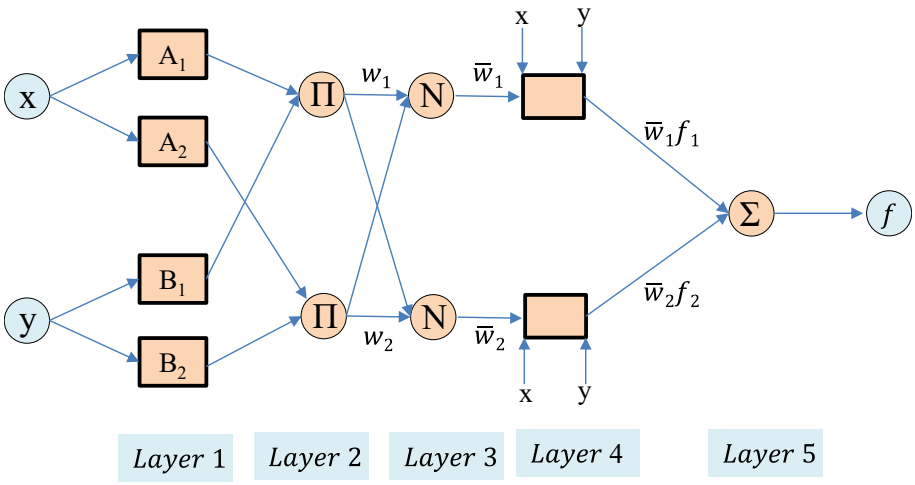

Fig. 5. Basic architecture of an ANFIS algorithm for two input variables.

In Eq. (7), w_i is firing strength of a rule.

Layer 3: Each node in this layer, which is called the normalization layer, is determined by the ratio of each the node's weight to the sum of the nodes' weights. $o_{l,23}$ is shown in Eq. (8).

$$o_{l,3} = \overline{w_i} = \frac{w_i}{w_1 + w_2 + \cdots + w_n} içini = 1, 2, \cdots., n \tag{8}$$

In Eq. (8), $\overline{w_i}$ is normalized firing strength.

Layer 4: Each node in this layer, which is referred to as the defuzzification layer, is determined by multiplying the node function with the normalized output. Results obtained from this layer ($o_{l,4}$) is shown in Eq. (9).

$$o_{l,4} = \overline{w_i} f_i = \overline{w_i}.(p_i.x + q_i.x + r_i) içini = 1, 2, .., n \tag{9}$$

In Eq. (9), p_i, q_i and r_i are consequent parameters.

Layer 5 (Output layer): This layer called summation layer consists of a single node that generates the summation of all incoming signals from preceding layers. Results obtained from this layer ($o_{l,5}$) is shown in Eq. (10).

$$o_{l,5} = \sum_i \overline{w_i} f_i = \frac{\sum_i w_i f_i}{\sum_i w_i} içini = 1, 2, \cdots., n \tag{10}$$

5. Experimental design and model parameters

To model the cement mortar samples' compressive strength, two ANN and two ANFIS models were developed. In the models, the following five parameters including age of samples (days), PC, pumice, diatomite and water were considered as the input parameters of ANN and ANFIS models. The cement mortar samples' compressive strength is the output. The input and output quantities used in ANN and ANFIS models are given in Table 4. In these models, 168 data obtained from experimental results were used for the training of the models. According to the TS EN 196-1 standard, the compressive strength test result is calculated as the arithmetic average of six different results obtained from six determinations made on three prism sets [42]. Therefore, 28 experimental data, which are determined by the average of six mortar samples produced for each cement, were used for testing models.

Table 4
The range of variables of ANN and ANFIS models.

Variable properties	Variables	Minimum	Maximum
Input	Age of samples (days)	2	90
	PC (g)	360	450
	Pumice (g)	0	90
	Diatomite (g)	0	90
	Water (g)	225	270
Output	Compressive strength, MPa	17.4	62.7

Two statistical methods were used to analyse the effect of each input variable of the ANN. In the first, the sensitivity levels of the input variables are computed by using SPSS 22.0 software package and correlations of the aforementioned variables are shown in Fig. 6. In the second, correlations between model parameters and variance inflation factor (VIF) values have been determined, and the results have been shown in Table 5.

When Fig. 6 is examined, it is seen that the "time" variable has a very important contribution to the output variables. It is also seen that the contribution of other input variables is approximately equal.

According to Table 5, when the correlation between the input variables is examined, it can be stated that there is a significant relationship between each other except for the diatomite variable ($c < 0.8$). However, it is seen that the degree of relationship between diatomite variable and water is low ($c = 0.996$). According to the relationship between compressive strength, which is the output variable, and the input variables, the highest correlation is between time variable ($c = 0.835$); the lowest correlation is between diatomite variable ($c = -0.172$). When the VIF is examined, it is seen that there is a one-to-one multicollinearity relationship between the time input variable and the output variable (Time VIF = 1), while there are nonlinear relationships between the diatomite input variables (30 < VIF). These results show that the choice of ANN, which is a model that does not consider linear relationships, is correct. According to both statistical methods, it can be said that the hydration age (day) input variable has a very important contribution to the output variables.

ANN models, called ANN-1 and ANN-2, consists of a feedforward backpropagation neural network (Fig. 7-a) and Elman backpropagation neural network (Fig. 7-b), respectively. Training parameter values of ANN models are given in Table 6.

To avoid overfitting, the training process was terminated at different times during the training of the ANN models.

In the creation of ANFIS models, determining the properties of membership functions is of primary importance for the success of the model. To determine these features optimally, a literature review was made, and studies on similar subjects were examined. As a result of the research, different epochs and learning algorithms were tried by choosing two different membership functions as "tri" (triangular-shaped) and "Psig" (product of two sigmoidal). The shape of fuzzy sets is preferred over the change of the crisp values and the membership function degree of the set. For example, if the change is linear, a triangular or trapezoidal membership function may be preferred. While

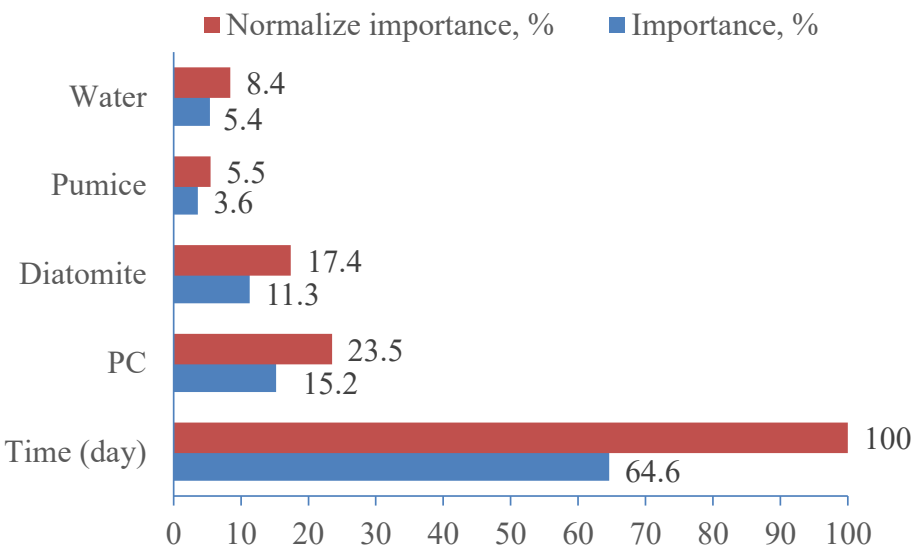

Fig. 6. Degree of importance of the input variables.

Table 5
Correlations between model parameters with VIF values.

Pearson Correlation	Compressive strength, MPa	Time (day)	PC (g)	Diatomite (g)	Pumice (g)	Water (g)	Statistics (VIF)
Compressive strength, MPa	1.000	0.835	0.242	−0.172	−0.072	−0.166	
Time (day)	0.835	1.000	0.000	0.000	0.000	0.000	1
PC (g)	0.242	0.000	1.000	−0.505	−0.505	−0.495	119.643
Diatomite (g)	−0.172	0.000	−0.505	1.000	−0.489	0.996	
Pumice (g)	−0.072	0.000	−0.505	−0.489	1.000	−0.496	119.739
Water (g)	−0.166	0.000	−0.495	0.996	−0.496	1.000	118.095

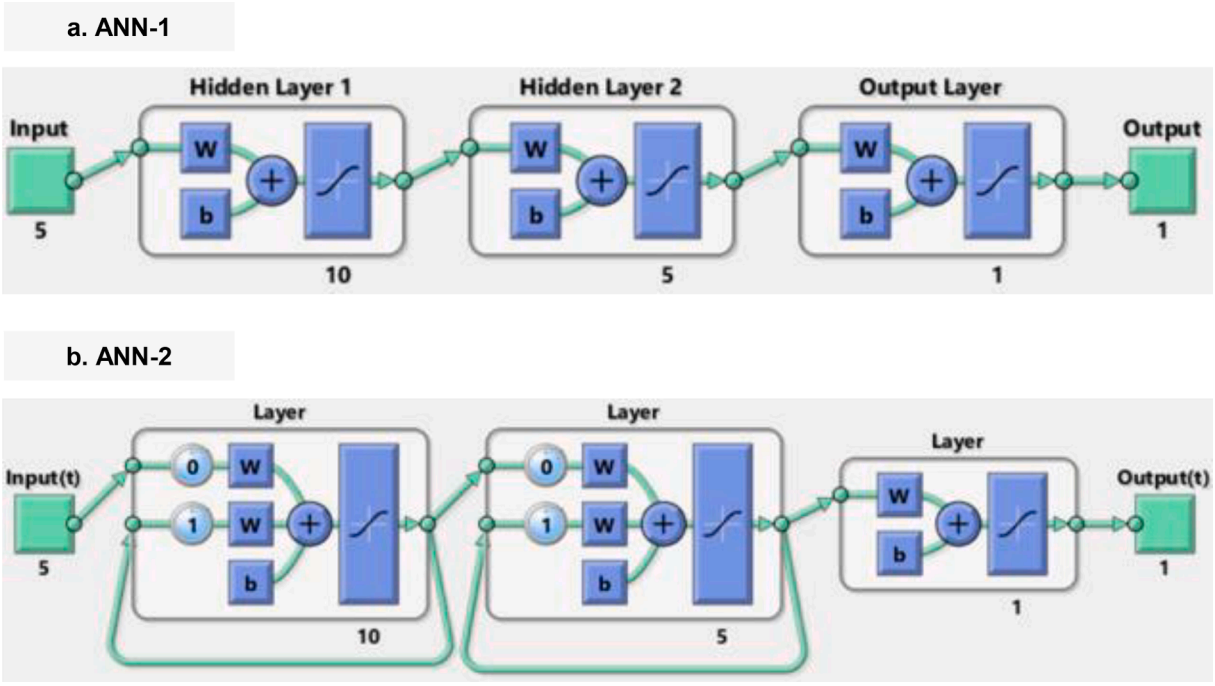

Fig. 7. The architecture of ANN models for compressive strength.

determining the shape of the fuzzy set, it is used according to empirical data or professional experience. If the appropriate membership function is selected, the training performance will be high [52]. The total parameter values of the selected ANFIS 1 and 2 models are given in Table 7. In addition, the membership functions of the inputs of the ANFIS-1 and 2 models are depicted in Figs. 8 and 9, respectively.

Table 6
Training parameter values of ANN models.

Parameter values	ANN-1	ANN-2
Input layer neuron numbers	5	5
Layer numbers	3	3
Hidden layer numbers	2	2
First hidden layer neuron numbers	10	10
Second hidden layer neuron numbers	5	5
Output layer neuron number	1	1
Epoch numbers	37	41
Learning cycle	0	6
Error after learning	$6.13x10^{-10}$	2.17

Table 7
The parameter values of ANFIS models.

Parameters	**ANFIS-1**	**ANFIS-2**
Structure of fuzzy	Sugeno	Sugeno
Output membership shape	Constant	Constant
Input membership shape	Tri	Psig
Input numbers	5	5
Output number	1	1
Total parameter numbers	288	303
Nodes	524	524
Linear parameter numbers	243	243
Nonlinear parameter numbers	45	60
Training data pair numbers	168	168
Fuzzy rule numbers	243	243
ANFIS training start error	2.42	1.5
Error after learning	2.34	1.5
Epochs	300	300

6. Results and discussion

In the training and testing stages, the comparison between the compressive strengths data obtained from the experiments and predicted values obtained from the ANN-1 and ANN-2 models are depicted in Figs. 10 and 11, respectively.

In the testing stages, the comparison between the compressive strengths data obtained from the experiments and predicted values obtained from the ANFIS-1 and ANFIS-2 models are depicted in Fig. 12.

The accuracy of the developed network models has been evaluated with three performance indicators. The performance indicators are coefficient of determination (R^2), a root-mean squared error (RMSE) and mean absolute percentage error (MAPE), and, they are calculated with the following Equations [53,54].

$$R^2 = 1 - \frac{\sum_{i=1}^{N}(y_i - r_i)^2}{\sum_{i=1}^{N}(r_i - y_m)^2} \tag{11}$$

$$RMSE = \sqrt{\frac{1}{N}\sum_{i=1}^{N}(y_i - r_i)^2} \tag{12}$$

$$MAPE = \frac{100}{n}\sum_{i=1}^{N}\left|\frac{r_i - y_i}{r_i}\right| \tag{13}$$

In the Equations: N = total number data; y_i = predicted data; r_i = actual data; y_m = average of the actual data.

Statistical data calculated in the training and testing stages of ANN-1 and ANN-2 models are depicted in Figs. 13 and 14, respectively. Statistical data in the test stages of ANFIS-1 and ANFIS-2 models are depicted in Fig. 15.

The R^2, RMSE and MAPE results of the ANN-1 (Fig. 13-a) and ANN-2 (Fig. 13-b) models in the training process were calculated as (0.9995,

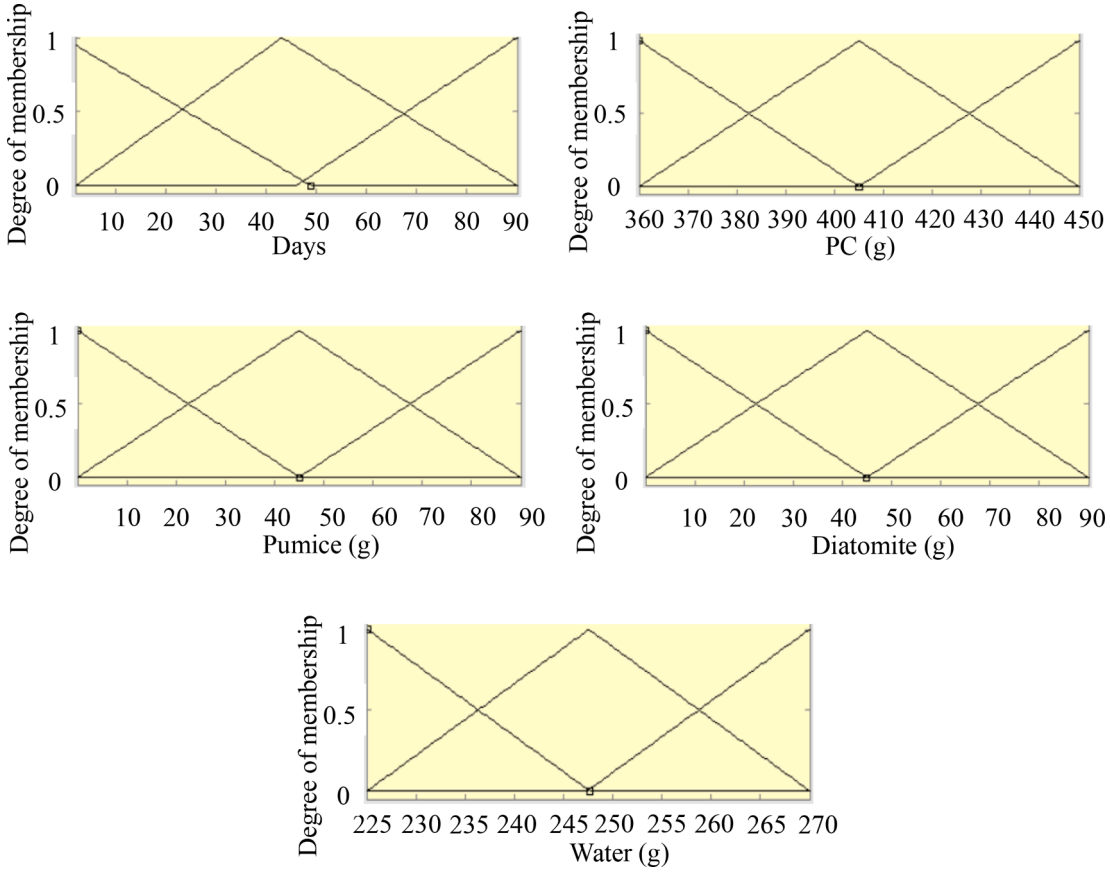

Fig. 8. Shapes of membership functions for the input variables of ANFIS-1 models.

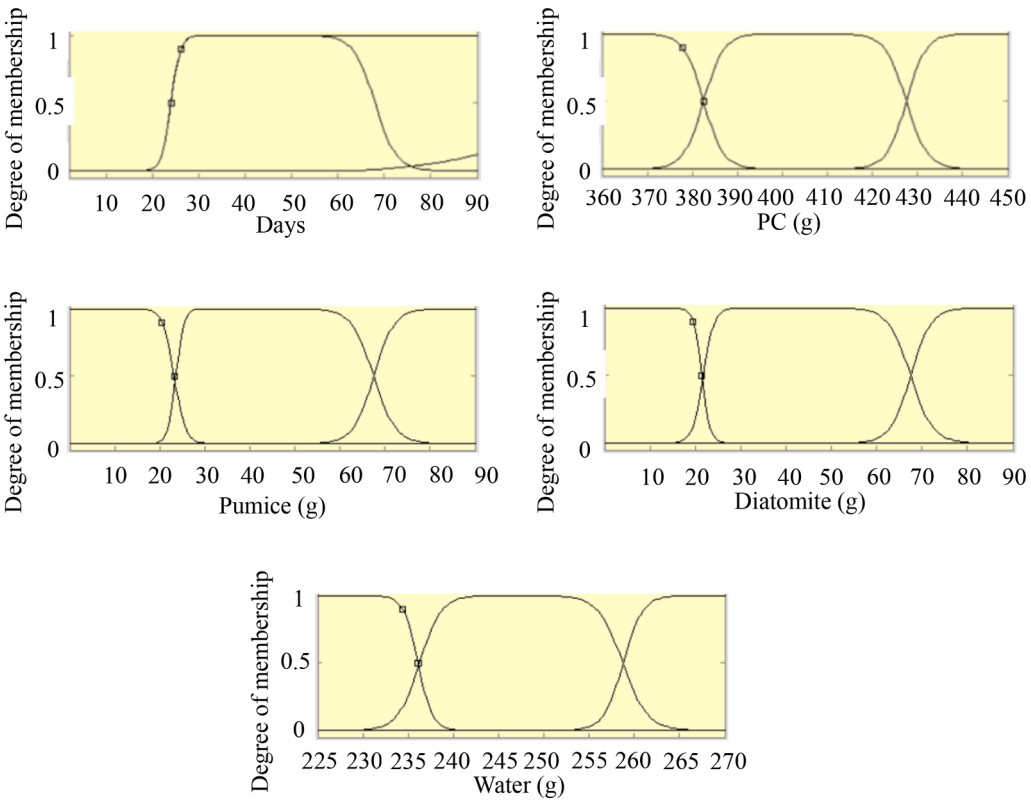

Fig. 9. Shapes of membership functions for the input variables of ANFIS-2 models.

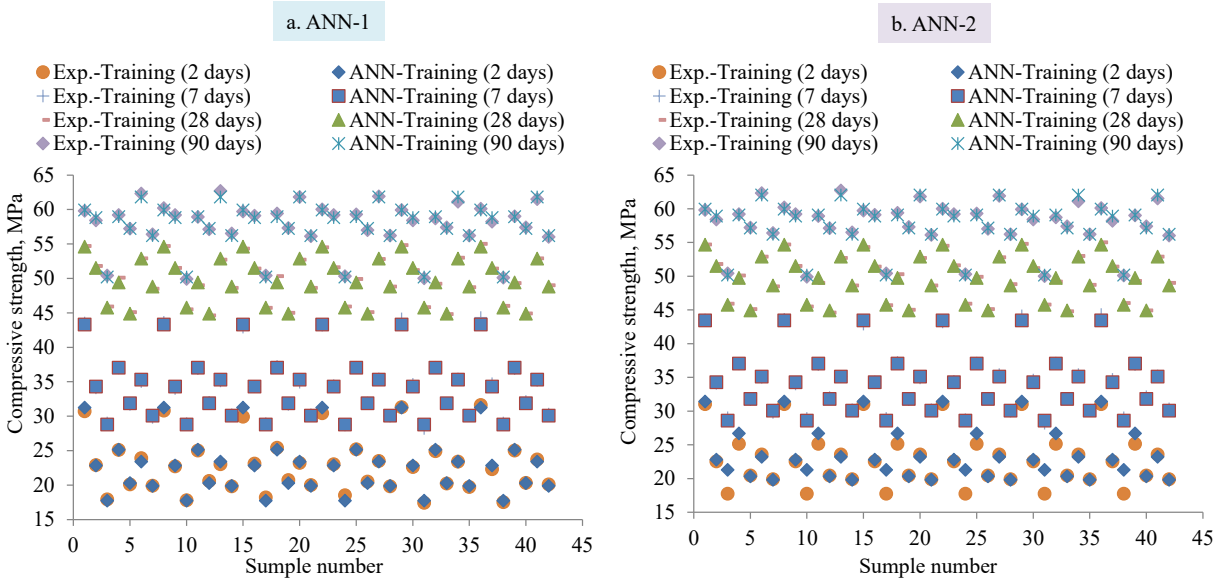

Fig. 10. Comparison of predicted values obtained from ANN models with actual values during the training stages.

0.9995), (0.3101, 0.3016) and (0.0064, 0.0066), respectively. During the testing process, the R^2, RMSE and MAPE results of the ANN-1 (Fig. 14-a) and ANN-2 (Fig. 14-b) models were calculated as (0.9999, 0.9999), (0.1295, 0.1077) and (0.0024, 0.0025), respectively. The R^2, RMSE and MAPE results of the ANFIS-1 (Fig. 15-a) and ANFIS-2 (Fig. 15-b) models in the testing process were calculated as (0.9723, 0.9889), (2.3271, 1.4777) and (0.0607, 0.0360), respectively.

Considering the R^2 value in the ANN and ANFIS models, it is seen that these values are very close to one. It can be stated that the estimated compressive strength values strongly reflect the truth, even in the ANFIS-1 model which has the smallest R^2 (0.9723) value. When the RMSE values in all models are taken into account, it is seen that these values are very close to zero. This shows that the estimated results are very close to the actual compressive strength values. The MAPE results in both ANN and ANFIS models are below 10%, indicating that these models have a "high accuracy" rating or can be classified as "very good". It can be stated that the cement mortar samples' compressive strength can be estimated with an accuracy of 99.75% with the ANN-2 model and 96.40% with the ANFIS-2 model, according to these results. Considering all the statistical indices in both the training and testing processes, it can

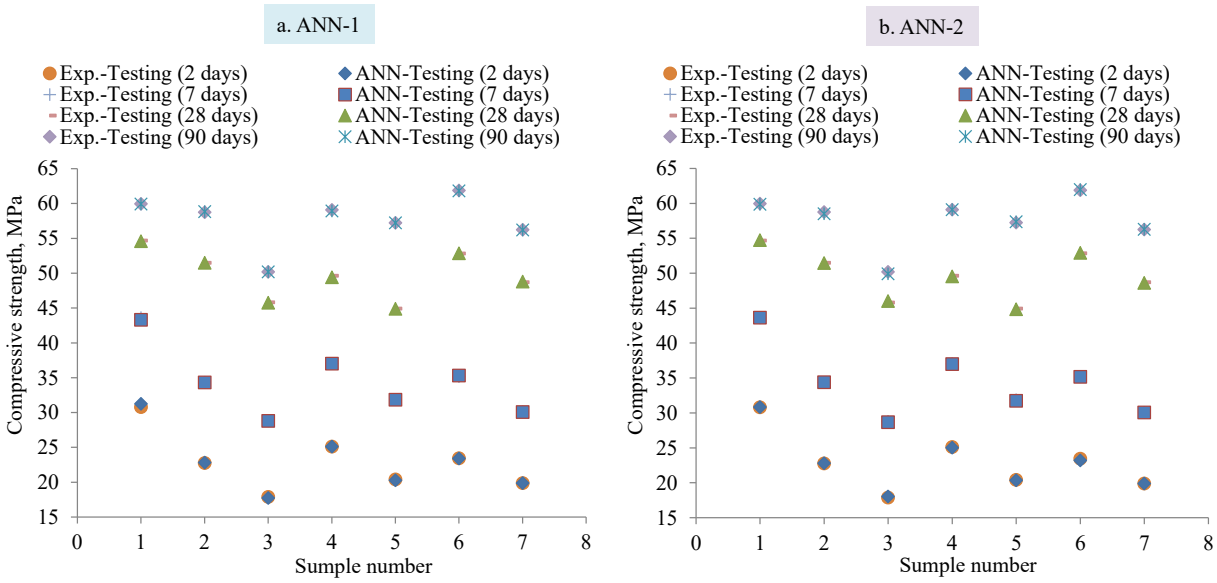

Fig. 11. Comparison of predicted values obtained from ANN models with actual values during testing stages.

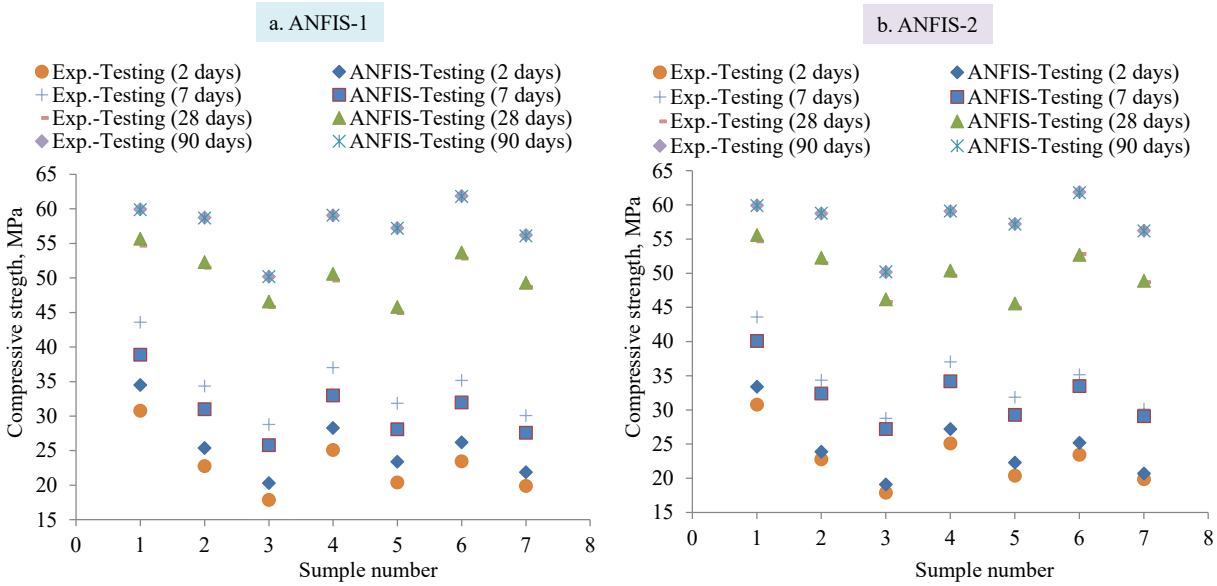

Fig. 12. Comparison of predicted values obtained from ANFIS models with actual values during the testing stages.

be stated that the compressive strength estimates at age of 2, 7, 28 and 90-days obtained from the ANN model are very close to the real values. The high performance of ANN models in the training process made us very nervous about overfitting. However, the high-performance results of the test data relieved us and made us think that there was no overfitting process. We thought that the reason for the high learning performance was due to the not too much data and also the fact that the "Date" input variable had a very high effect on the output, as seen in Fig. 6.

To evaluate the effectiveness of these models, the results have been compared with error measurements from previous studies in this area (Table 8).

When the data obtained are compared with the models in other studies in the field (Table 8), it can be stated that the ANN and ANFIS models are positive.

To examine each test result one by one and to see the errors more clearly, the actual values on the hydration days and the compressive strength values estimated by the ANN and ANFIS models were compared. Compressive strength values at age of 2-day are depicted in Fig. 16, and errors with percentage differences among the results are given in Table 9.

According to the actual compressive strength values of the cement mortar samples at age of 2-day, the highest value with 30.78 MPa in the R coded mortar, while the smallest value of 17.88 MPa in the D20 coded mortar was obtained (Fig. 16). Furthermore, it was determined that the most change was in the ANFIS-1 model with 12.82% percent difference and −3.00 MPa error in P20 coded mortar, and the least change was in the ANN-1 model with 0.0% percent difference and 0.0 MPa error in P10D10 coded mortar (Table 9).

Compressive strength values at age of 7-day are depicted in Fig. 17, and errors with percentage differences among the results are given in Table 10.

According to the actual compressive strength values of the cement mortar samples at age of 7-day, the highest value with 43.60 MPa in the

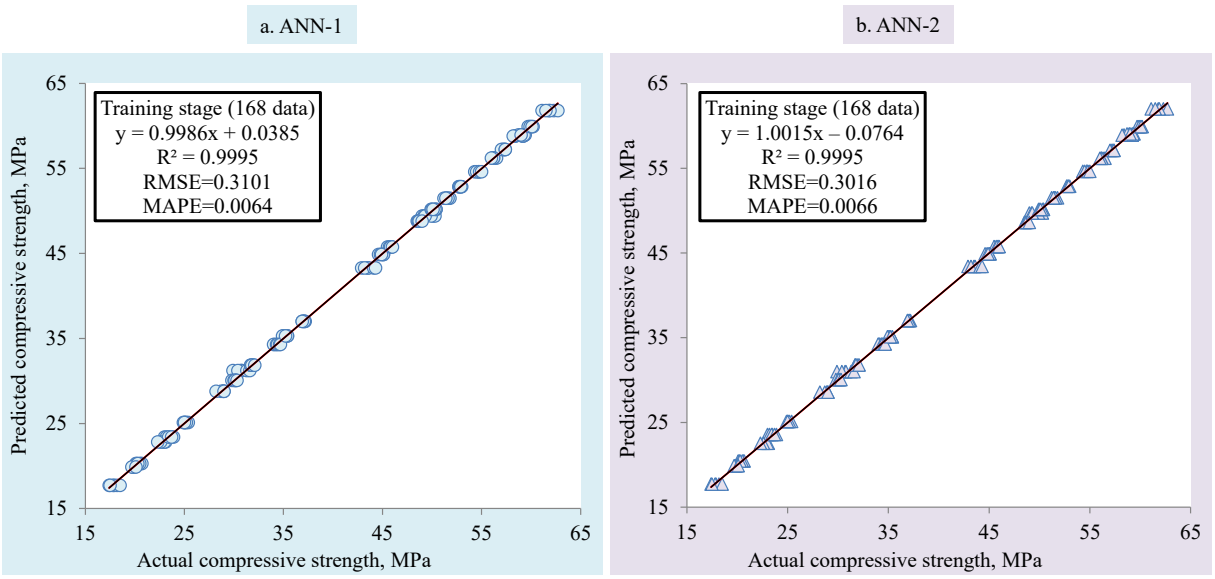

Fig. 13. Statistical properties of the data in the training process in the ANN models.

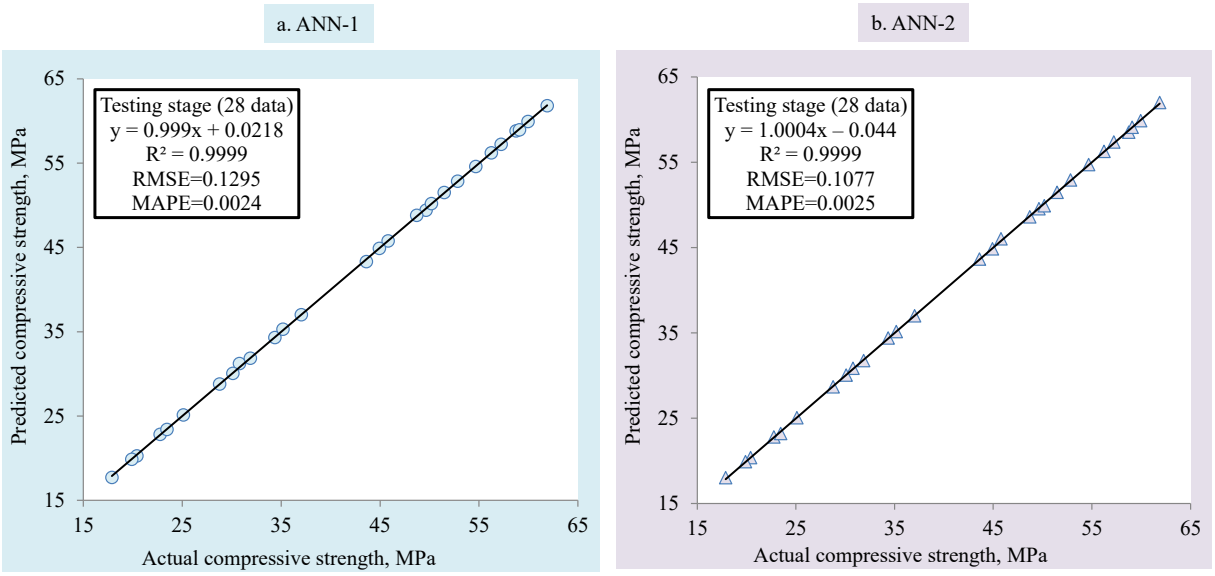

Fig. 14. Statistical properties of the data in the testing process in the ANN models.

R coded mortar, while the smallest value of 28.78 MPa in the 20D coded mortar was obtained (Fig. 17). Furthermore, it was determined that the most change was in the ANFIS-1 model with 13.40% percent difference and 3.77 MPa error in P20 coded mortar, and the least change was in the ANN-2 model with 0.0% percent difference and 0.0 MPa error in P10 coded mortar (Table 10).

Compressive strength values at age of 28-day are depicted in Fig. 18, and errors with percentage differences among the results are given in Table 11.

According to the actual compressive strength values of the cement mortar samples at age of 28-day, the highest value with 54.67 MPa in the R coded mortar, while the smallest value of 44.92 MPa in the P20 coded mortar was obtained (Fig. 18). Furthermore, it was determined that the most change was in the ANFIS-1 model with −1.93% percent difference and −0.88 MPa error in P20 coded mortar, and the least change was in the ANN-1 model with 0.01% percent difference and 0.01 MPa error in R coded mortar (Table 11).

Compressive strength values at age of 90-day are depicted in Fig. 19, and errors with percentage differences among the results are given in Table 12.

According to the actual compressive strength values of the cement mortar samples at age of 90-day, the highest value with 59.95 MPa in the R coded mortar, while the smallest value of 50.18 MPa in the D20 coded mortar was obtained (Fig. 19). Furthermore, it was determined that the most change was in the ANN-2 model with −0.29% percent difference and −0.17 MPa error in D10 coded mortar, and the least change was in the ANN-1 and ANN-2 models with 0.0% percent difference and 0.0 MPa error in D20 and R coded mortar samples (Table 12).

Observed results imply that both ANN and ANFIS models yield highly accurate prediction performance. Particularly, ANN introduces the best prediction performance and minimum error rates.

7. Conclusion

In this study, two ANN and two ANFIS models were exploited for the prediction at age of 2, 7, 28, and 90-days compressive strength of the

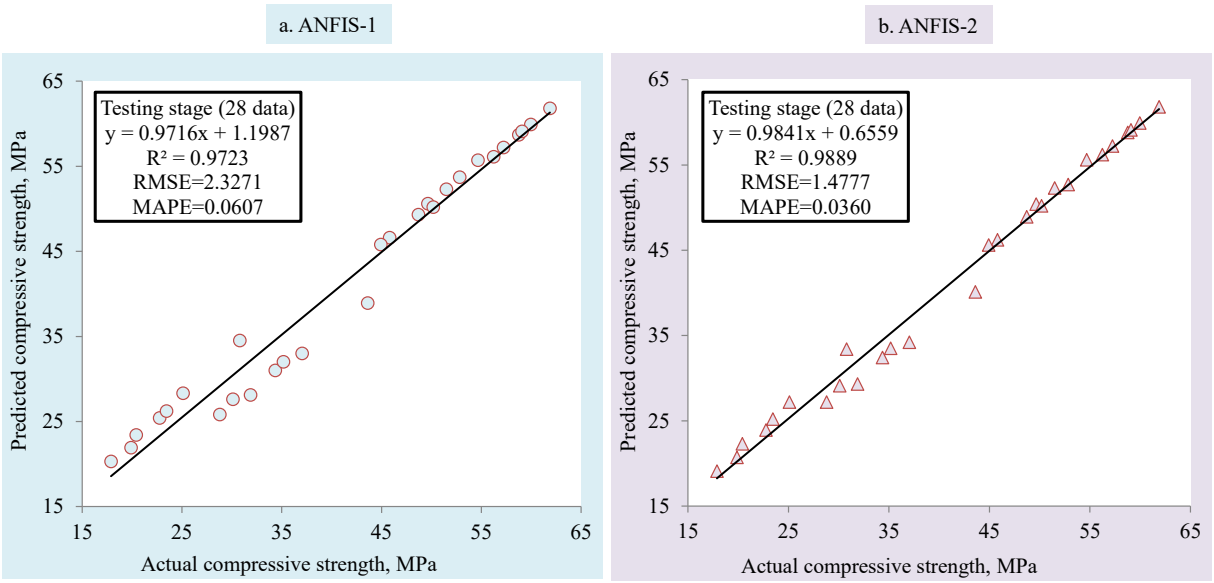

Fig. 15. Statistical properties of the data in the testing process in the ANFIS models.

Table 8
Error measurements for predicting compressive strength in the testing process in the ANN and ANFIS models suggested by other researchers.

References	Models	R^2	RMSE	MAPE
Present study	ANN-1	0.9999	0.1295	0.0024
	ANN-2	0.9999	0.1077	0.0025
	ANFIS-1	0.9723	2.3271	0.0607
	ANFIS-2	0.9889	1.4777	0.0360
[3]	ANN	0.8600	4.3800	0.0333
	ANFIS	0.9600	2.3700	0.0199
[24]	ANN	0.9974	1.2315	0.4200
[27]	ANN	0.9743	2.7400	0.0563
	ANFIS	0.9909	2.0975	0.0516
[54]	ANN	0.9976	0.3521	0.0042
	ANFIS	0.9879	0.7827	0.1060
[55]	ANN	–	1.7000	0.0241
	ANFIS	–	0.0400	0.00027
[56]	ANN	0.9700	6.7000	0.0498
[57]	ANN	0.9970	0.9260	–
	ANFIS	0.9980	0.8240	–
[58]	ANN	0.9357	14.370	–
	ANFIS	0.9483	0.0003	–
[59]	ANN	0.9438	8.7100	–
	ANFIS	0.9518	10.900	–
[60]	ANN	0.8510	2.4230	0.0199
	ANFIS	0.8790	2.2650	0.0165

seven different cement mortars, which contain pumice and/or diatomite. While developing these four models, 168 data were used for training, and 28 data were used for testing.

According to the findings from the study;

- According to SEM images, diatomite and pumice contain porous structures. Moreover, while diatomite has micropores structures of different sizes and shapes, pumice has an irregular plate shape and irregular morphology.
- According to the XRD results, PC has a crystalline structure, while Pumice and diatomite have amorphous structures composed of quartz (SiO_2).
- According to the FT-IR results, pumice and diatomite are mainly composed of SiO_2 and appeared to have a similar structure to those reported in the literature.
- According to chemical analysis, pumice and diatomite have the properties specified in the standards for a natural pozzolan and are positive for pozzolanic properties ($SiO_2 + Al_2O_3 + Fe_2O_3 > 70\%$).
- As a result of the particle size analysis, the particles of zeolite are coarse, the ones of PC are medium and the ones of diatomite are fine.
- When specific gravities and Blaine values are considered, 3.18 g/cm^3 and 3822 cm^2/g for PC, 2.70 g/cm^3 and 2645 cm^2/g for pumice, and 2.58 g/cm^3 and 6112 cm^2/g for diatomite, respectively. Therefore, diatomite has the lowest specific gravity and the highest Blaine value.
- The compressive strength values of cement mortar samples vary depending on the pozzolanic material type, substitution rate and hydration time. While pumice and/or diatomite substituted mortars show significant losses in compressive strength on the 2-day and 7-day, they continuously increase in compressive strength especially on 28-day and 90-day. The healing effect on the compressive strength of pumice and/or diatomite shows up mainly on the 90-day. Obtained experimental data showed that pumice and/or diatomite had lower pozzolanic activity at early ages, but increased pozzolanic activity at later ages. This, in turn, led to an increase in compressive strength at later ages. In addition, it was determined that the compressive strength values of all mortar samples containing 10% and 20% pumice or diatomite at 28-day were above the minimum value of 42.5 MPa specified in the TS EN 197-1 standard. These results show that it will save up to 20% from Portland cement. Moreover, at 90-day, the compressive strength of P5D5 coded cement mortars has been obtained higher than that of the reference cement mortar.
- When comparing the prediction and the experimental values in the testing stage R^2, RMS and MAPE were found as 0.9999, 0.1295, 0.0024 for ANN-1, 0.9999, 0.1077, 0.0025 for ANN-2, 0.9723, 2.3271, 0.0607 for ANFIS-1, 0.9889, 0.1477, 0.0360 for ANFIS-2, respectively.

According to the data obtained, it has been seen that these models can make very good predictions for cement mortars' compressive strength values. For this reason, it can be said that the compressive strength of these cement mortars can be estimated with a very small error and in a short time with both ANN and ANFIS models. However, the experimental studies in this study are limited to pumice and/or diatomite and only CEM I 42.5 R type Portland cement. This caused the prediction results to be so good. In future studies, more inclusive results

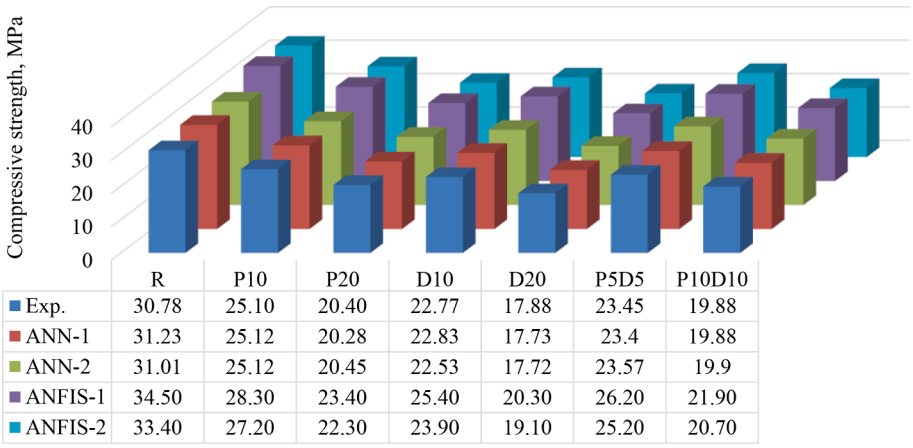

Fig 16. Comparison of compressive strength values at age of 2-day.

Table 9
Comparison of errors among compressive strength values at age of 2-day.

Cement coded	ANN-1		ANN-2		ANFIS-1		ANFIS-2	
	Error, MPa	Percentage difference, %	Error, MPa	Percentage difference, %	Error, MPa	Percentage difference, %	Error, MPa	Percentage difference, %
R	−0.45	−1.43	−0.23	−0.73	−3.72	−10.77	−2.62	−7.83
P10	−0.02	−0.08	−0.02	−0.08	−3.20	−11.31	−2.10	−7.72
P20	0.12	0.59	−0.05	−0.24	−3.00	−12.82	−1.90	−8.52
D10	−0.06	−0.28	0.24	1.05	−2.63	−10.37	−1.13	−4.74
D20	0.15	0.86	0.16	0.92	−2.42	−11.90	−1.22	−6.37
P5D5	0.05	0.21	−0.12	−0.51	−2.75	−10.50	−1.75	−6.94
P10D10	0.00	0.00	−0.02	−0.08	−2.02	−9.21	−0.82	−3.95

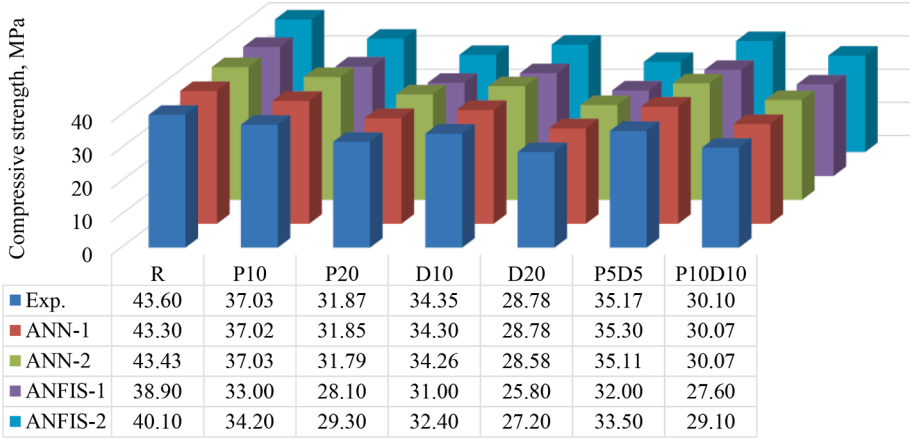

Fig. 17. Comparison of compressive strength values at age of 7-day.

Table 10
Comparison of errors among ocompressive strength values at age of 7-day.

Cement coded	ANN-1		ANN-2		ANFIS-1		ANFIS-2	
	Error, MPa	Percentage difference, %	Error, MPa	Percentage difference, %	Error, MPa	Percentage difference, %	Error, MPa	Percentage difference, %
R	0.30	0.69	0.17	0.39	4.70	12.08	3.50	8.73
P10	0.01	0.04	0.00	0.00	4.03	12.22	2.83	8.28
P20	0.02	0.05	0.08	0.24	3.77	13.40	2.57	8.76
D10	0.05	0.15	0.09	0.26	3.35	10.81	1.95	6.02
D20	0.00	0.00	0.20	0.71	2.98	11.56	1.58	5.82
P5D5	−0.13	−0.38	0.06	0.16	3.17	9.90	1.67	4.98
P10D10	0.03	0.10	0.03	0.10	2.50	9.06	1.00	3.44

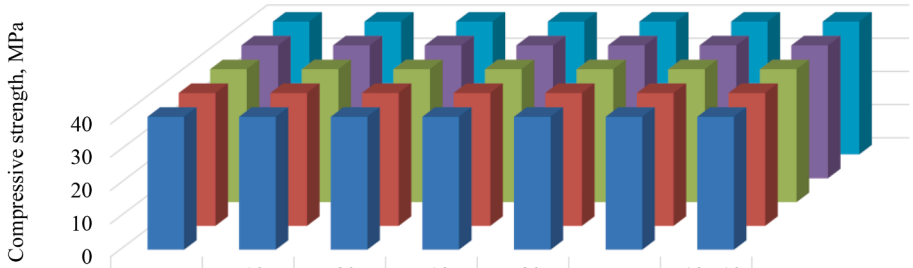

	R	P10	P20	D10	D20	P5D5	P10D10
Exp.	54.67	49.63	44.92	51.48	45.80	52.83	48.70
ANN-1	54.60	49.40	44.88	51.50	45.76	52.85	48.80
ANN-2	54.66	49.74	44.90	51.52	45.77	52.89	48.62
ANFIS-1	55.70	50.60	45.80	52.30	46.60	53.70	49.30
ANFIS-2	55.60	50.40	45.60	52.30	46.20	52.70	48.90

Fig. 18. Comparison of compressive strength r values at age of 28-day.

Table 11
Comparison of errors among compressive strength values at age of 28-day.

Cement coded	ANN-1		ANN-2		ANFIS-1		ANFIS-2	
	Error, MPa	Percentage difference, %	Error, MPa	Percentage difference, %	Error, MPa	Percentage difference, %	Error, MPa	Percentage difference, %
R	0.07	0.12	0.01	0.01	−1.03	−1.86	−0.93	−1.68
P10	0.23	0.47	−0.11	−0.21	−0.97	−1.91	−0.77	−1.52
P20	0.04	0.08	0.02	0.04	−0.88	−1.93	−0.68	−1.50
D10	−0.02	−0.03	−0.04	−0.07	−0.82	−1.56	−0.82	−1.56
D20	0.04	0.09	0.03	0.07	−0.80	−1.72	−0.40	−0.87
P5D5	−0.02	−0.03	−0.06	−0.11	−0.87	−1.61	0.13	0.25
P10D10	−0.10	−0.20	0.08	0.16	−0.60	−1.22	−0.20	−0.41

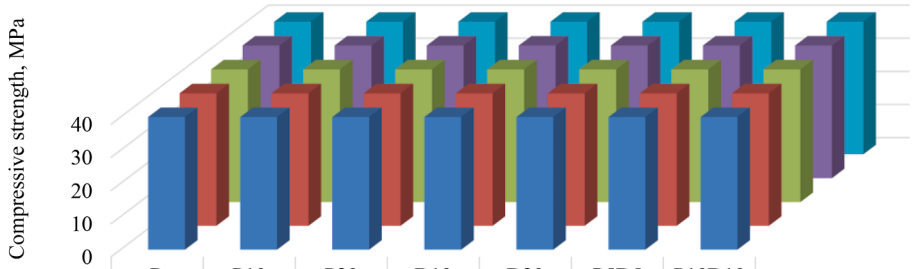

	R	P10	P20	D10	D20	P5D5	P10D10
Exp.	59.95	59.08	57.23	58.75	50.18	61.88	56.23
ANN-1	59.93	58.93	57.23	58.82	50.18	61.80	56.21
ANN-2	59.95	59.07	57.13	58.92	50.16	62.04	56.21
ANFIS-1	59.90	59.10	57.20	58.70	50.20	61.80	56.10
ANFIS-2	59.90	59.10	57.20	58.80	50.20	61.80	56.20

Fig. 19. Comparison of compressive strength values at age of 90-day.

Table 12
Comparison of errors among compressive strength values at age of 90-day.

Cement coded	ANN-1		ANN-2		ANFIS-1		ANFIS-2	
	Error, MPa	Percentage difference, %	Error, MPa	Percentage difference, %	Error, MPa	Percentage difference, %	Error, MPa	Percentage difference, %
R	0.02	0.03	0.00	0.00	0.05	0.08	0.05	0.08
P10	0.15	0.26	0.01	0.02	−0.02	−0.03	−0.02	−0.03
P20	0.00	0.01	0.10	0.18	0.03	0.06	0.03	0.06
D10	−0.07	−0.12	−0.17	−0.29	0.05	0.09	−0.05	−0.09
D20	0.00	0.00	0.02	0.05	−0.02	−0.03	−0.02	−0.03
P5D5	0.08	0.13	−0.16	−0.25	0.08	0.13	0.08	0.13
P10D10	0.02	0.04	0.02	0.04	0.13	0.24	0.03	0.06

can be obtained by developing these models with other cement types and different supplementary cementitious materials.

CRediT authorship contribution statement

Burak Kocak: . **İbrahim Pınarcı:** . **Uğur Güvenç:** Supervision. **Yilmaz Kocak:** .

Declaration of Competing Interest

The authors declare that they have no known competing financial interests or personal relationships that could have appeared to influence the work reported in this paper.

Data availability

All data, models and code used during the study are available in the submitted manuscript.

Acknowledgement

Material analyses carried out for this study were supported by Duzce University Research Fund (Project Code No: 2021.06.08.1190). In addition, the authors would like to thank the Eskisehir CIMSA cement factory managers and employees for their invaluable contributions to the performance of compressive strength tests.

References

[1] L. Imtiaz, S. K. U. Rehman, S. Ali Memon, M. Khizar Khan, & M. Faisal Javed, A review of recent developments and advances in eco-friendly geopolymer concrete, Applied Sciences, 10(21) (2020) 7838, https://doi.org/10.3390/app10217838.
[2] A.A. Aliabdo M. Abd Elmoaty M.A. Emam Factors affecting the mechanical properties of alkali activated ground granulated blast furnace slag concrete Construction and Building Materials 197 (2019) 339 355 10.1016/j.conbuildmat.2018.11.086.
[3] M.N. Amin, M.F. Javed, K. Khan, F.I. Shalabi, M.G. Qadir, Modeling Compressive Strength of Eco-Friendly Volcanic Ash Mortar using Artificial Neural Networking, Symmetry 13 (11) (2021) 2009, https://doi.org/10.3390/sym13112009.
[4] A.R. Kushnir, M.J. Heap, L. Griffiths, et al., The fire resistance of high-strength concrete containing natural zeolites, Cem. Concr. Compos. 103897 (2021), https://doi.org/10.1016/j.cemconcomp.2020.103897.
[5] İ. Pınarcı, Y. Kocak, Hydration mechanisms and mechanical properties of pumice substituted cementitious binder, Constr. Build. Mater. 335 (2022), 127528, https://doi.org/10.1016/j.conbuildmat.2022.127528.
[6] M. Sun, C. Zou, D. Xin, Pore structure evolution mechanism of cement mortar containing diatomite subjected to freeze-thaw cycles by multifractal analysis, Cem. Concr. Compos. 103731 (2020), https://doi.org/10.1016/j.cemconcomp.2020.103731.
[7] A. Joshaghani, The effect of trass and fly ash in minimizing alkali-carbonate reaction in concrete, Constr. Build. Mater. 150 (2017) 583–590, https://doi.org/10.1016/j.conbuildmat.2017.06.034.
[8] G. Adil, J.T. Kevern, D. Mann, Influence of silica fume on mechanical and durability of pervious concrete, Constr. Build. Mater. 118453 (2020), https://doi.org/10.1016/j.conbuildmat.2020.118453.
[9] Y.J. Lee, H.G. Kim, K.H. Kim, Effect of Ground Granulated Blast Furnace Slag Replacement Ratio on Structural Performance of Precast Concrete Beams, Materials 14 (23) (2021) 7159, https://doi.org/10.3390/ma14237159.
[10] S.K. Das, J. Mishra, S.M. Mustakim, A. Adesina, C.R. Kaze, D. Das, Sustainable utilization of ultrafine rice husk ash in alkali activated concrete: Characterization and performance evaluation, J. Sustain. Cem.-Based Mater. 11 (2) (2022) 142–160, https://doi.org/10.1080/21650373.2021.1894265.
[11] M.M.A. Elahi, C.R. Shearer, A.N.R. Reza, A.K. Saha, M.N.N. Khan, M.M. Hossain, P. K. Sarker, Improving the sulfate attack resistance of concrete by using supplementary cementitious materials (SCMs): A review, Constr. Build. Mater. 281 (2021), 122628, https://doi.org/10.1016/j.conbuildmat.2021.122628.
[12] J. Liu, K. Wu, Y. Wang, Y. Yang, Effects of fly ash/diatomite admixture with variable particle sizes on the mechanical properties and porosity of concrete, Journal of Wuhan University of Technology-Mater, Sci. Ed. 32 (5) (2017) 1072–1079, https://doi.org/10.1007/s11595-017-1713-8.
[13] M. Askarian, S. Fakhretaha Aval, & A. Joshaghani, A comprehensive experimental study on the performance of pumice powder in self-compacting concrete (SCC), Journal of Sustainable Cement-Based Materials, 7(6) (2018) 340-356, https://doi.org/10.1080/21650373.2018.1511486.
[14] M. Kurtay, H. Gerengi, Y. Kocak, M.A. Chidiebere, M. Yildiz, The potency of zeolite and diatomite on the corrosive destruction of reinforcing steel in 1 M HNO3 environment, Constr. Build. Mater. 236 (2020), 117572, https://doi.org/10.1016/j.conbuildmat.2019.117572.
[15] J. Liu, D. Wang, Influence of steel slag-silica fume composite mineral admixture on the properties of concrete, Powder Technol. 320 (2017) 230–238, https://doi.org/10.1016/j.powtec.2017.07.052.
[16] M. Tabish, M.M. Zaheer, A. Baqi, Effect of nano-silica on mechanical, microstructural and durability properties of cement-based materials: A review, Journal of Building, Engineering 105676 (2022), https://doi.org/10.1016/j.jobe.2022.105676.
[17] G. Pazouki, Fly ash-based geopolymer concrete's compressive strength estimation by applying artificial intelligence methods, Measurement 203 (2022), 111916, https://doi.org/10.1016/j.measurement.2022.111916.
[18] H. Nguyen, N.D. Hoang, Computer vision-based classification of concrete spall severity using metaheuristic-optimized Extreme Gradient Boosting Machine and Deep Convolutional Neural Network, Autom. Constr. 140 (2022), 104371, https://doi.org/10.1016/j.autcon.2022.104371.
[19] Q. Wang, A. Hussain, M.U. Farooqi, A.F. Deifalla, Artificial intelligence-based estimation of ultra-high-strength concrete's flexural property, Case Stud. Constr. Mater. 17 (2022) e01243.
[20] H.A. Al-Jamimi, W.A. Al-Kutti, S. Alwahaishi, K.S. Alotaibi, Prediction of compressive strength in plain and blended cement concretes using a hybrid artificial intelligence model, Case Stud. Constr. Mater. 17 (2022) e01238.
[21] M.M. Moein, A. Saradar, K. Rahmati, S.H.G. Mousavinejad, J. Bristow, V. Aramali, M. Karakouzian, Predictive models for concrete properties using machine learning and deep learning approaches: A review, Journal of Building, Engineering 105444 (2022), https://doi.org/10.1016/j.jobe.2022.105444.
[22] M.S. Sandeep, K. Tiprak, S. Kaewunruen, P. Pheinsusom, W. Pansuk, Shear strength prediction of reinforced concrete beams using machine learning, Structures 47 (2023) 1196–1211, https://doi.org/10.1016/j.istruc.2022.11.140.
[23] J. Xu, X. Zhao, Y. Yu, T. Xie, G. Yang, J. Xue, Parametric sensitivity analysis and modelling of mechanical properties of normal-and high-strength recycled aggregate concrete using grey theory, multiple nonlinear regression and artificial neural networks, Constr. Build. Mater. 211 (2019) 479–491, https://doi.org/10.1016/j.conbuildmat.2019.03.234.
[24] S. Chithra, S.S. Kumar, K. Chinnaraju, F.A. Ashmita, A comparative study on the compressive strength prediction models for High Performance Concrete containing nano silica and copper slag using regression analysis and Artificial Neural Networks, Constr. Build. Mater. 114 (2016) 528–535, https://doi.org/10.1016/j.conbuildmat.2016.03.214.
[25] A. Behnood, K.P. Verian, M.M. Gharehveran, Evaluation of the splitting tensile strength in plain and steel fiber-reinforced concrete based on the compressive strength, Constr. Build. Mater. 98 (2015) 519–529, https://doi.org/10.1016/j.conbuildmat.2015.08.124.
[26] E. Gulbandilar, Y. Kocak, Application of expert systems in prediction of flexural strength of cement mortars, Comput. Concr. 18 (1) (2016) 1–16, https://doi.org/10.12989/cac.2016.18.1.001.
[27] D.J. Armaghani, P.G. Asteris, A comparative study of ANN and ANFIS models for the prediction of cement-based mortar materials compressive strength, Neural Comput. & Applic. 33 (9) (2021) 4501–4532, https://doi.org/10.1007/s00521-020-05244-4.
[28] TS EN 197–1, Cement- Part 1: Compositions and conformity criteria for common cements", Turkish Standards 2012, Ankara–Turkey.
[29] A. Yucel, T. Efe, M. Onal, T. Depci, & H. Aydin, Mineralogical and chemical characterization of acidic pumices outcrop North of Lake Van, In IOP Conference Series: Earth and Environmental Science (2016, October) 052019) IOP Publishing, 10.1088/1755-1315/44/5/052019.
[30] A. Sarı, G. Hekimoğlu, V.V. Tyagi, R.K. Sharma, Evaluation of pumice for development of low-cost and energy-efficient composite phase change materials and lab-scale thermoregulation performances of its cementitious plasters, Energy (2020), 118242, https://doi.org/10.1016/j.energy.2020.118242.
[31] B. Figarska-Warchoł, G. Stańczak, M. Rembiś, & T. Tobola, Diatomaceous rocks of the Jawornik deposit (the Polish Outer Carpathians): petrophysical and petrographical evaluation, Geology, Geophysics and Environment, 41(4) (2015) 311–331, dx.doi.org/10.7494/geol.2015.41.4.311.
[32] K. Cabrera-Luna, E.E. Maldonado-Bandala, D. Nieves-Mendoza, P. Castro-Borges, P. Perez-Cortes, J.I. Escalante García, Supersulfated cements based on pumice with quicklime, anhydrite and hemihydrate: Characterization and environmental impact, Cem. Concr. Compos. 104236 (2021), https://doi.org/10.1016/j.cemconcomp.2021.104236.
[33] G. Yao, J. Lei, X. Zhang, Z. Sun, S. Zheng, S. Komarneni, Mechanism of zeolite X crystallization from diatomite, Mater. Res. Bull. 107 (2018) 132–138, https://doi.org/10.1016/j.materresbull.2018.07.021.
[34] C.E.M. Gomes, O.P. Ferreira, Analyses of microstructural proporties of va/veova copolymer modified cement pastes, Polimeros: Ciencia E Tecnologia 15 (3) (2005) 193–198, https://doi.org/10.1590/S0104-14282005000300009.
[35] C.E.M. Gomes, O.P. Ferreira, M.R. Fernandes, Influence of vinyl acetate–versatic vinylester copolymer on the microstructural characteristics of cement pastes, Material Research 8 (1) (2005) 51–56, https://doi.org/10.1590/S1516-14392005000100010.
[36] A. Govin, A. Peschard, R. Guyonnet, Modification of cement hydration at early ages by natural and heated wood, Cem. Concr. Compos. 28 (1) (2006) 12–20, https://doi.org/10.1016/j.cemconcomp.2005.09.002.
[37] M. Sarıdemir, M. Bulut, Effects of ground basaltic pumice and high temperatures on the properties of HSMs, Journal of Building, Engineering 102772 (2021), https://doi.org/10.1016/j.jobe.2021.102772.

[38] M.N. Sepehr, A. Amrane, K.A. Karimaian, M. Zarrabi, H.R. Ghaffari, Potential of waste pumice and surface modified pumice for hexavalent chromium removal: characterization, equilibrium, thermodynamic and kinetic study, J. Taiwan Inst. Chem. Eng. 45 (2) (2014) 635–647, https://doi.org/10.1016/j.jtice.2013.07.005.
[39] J.A.C. Costa, A.E. Martinelli, R. M. do Nascimento, & A. M. Mendes,, Microstructural design and thermal characterization of composite diatomite-vermiculite paraffin-based form-stable PCM for cementitious mortars, Constr. Build. Mater. 232 (2020), 117167, https://doi.org/10.1016/j.conbuildmat.2019.117167.
[40] T. Qian, J. Li, X. Min, Y. Deng, W. Guan, L. Ning, Diatomite: A promising natural candidate as carrier material for low, middle and high temperature phase change material, Energ. Conver. Manage. 98 (2015) 34–45, https://doi.org/10.1016/j.enconman.2015.03.071.
[41] TS 25, Natural pozzolan (Trass) for use in cement and concrete - Definitions, requirements and conformity criteria, Turkish Standards 2015, Ankara-Turkey.
[42] TS EN 196–1, Methods of testing cement–Part 1: Determination of strength. Turkish Standards 2002, Ankara–Turkey.
[43] E. Adesanya, A. Aladejare, A. Adediran, A. Lawal, M. Illikainen, Predicting shrinkage of alkali-activated blast furnace-fly ash mortar samples using artificial neural network (ANN), Cem. Concr. Compos. 124 (2021), 104265, https://doi.org/10.1016/j.cemconcomp.2021.104265.
[44] I. Mansouri, O. Kisi, Prediction of debonding strength for masonry elements retrofitted with FRP composites using neuro fuzzy and neural network approaches, Compos. B Eng. 70 (2015) 247–255, https://doi.org/10.1016/j.compositesb.2014.11.023.
[45] B. Wang, T. Man, H. Jin, Prediction of expansion behavior of self-stressing concrete by artificial neural networks and fuzzy inference systems, Constr. Build. Mater. 84 (2015) 184–191, https://doi.org/10.1016/j.conbuildmat.2015.03.059.
[46] M. Shariati, M.S. Mafipour, P. Mehrabi, A. Bahadori, Y. Zandi, M.N. Salih, H. Nguyen, J. Dou, X. Song, S. Poi-Ngian, Application of a hybrid artificial neural network-particle swarm optimization (ANN-PSO) model in behavior prediction of channel shear connectors embedded in normal and high-strength concrete, Appl. Sci. 9 (24) (2019) 5534, https://doi.org/10.3390/app9245534.
[47] A. Saradar, P. Nemati, A.S. Paskiabi, M.M. Moein, H. Moez, E.H. Vishki, Prediction of mechanical properties of lightweight basalt fiber reinforced concrete containing silica fume and fly ash: Experimental and numerical assessment, J. Build. Eng. 32 (2020), 101732, https://doi.org/10.1016/j.jobe.2020.101732.
[48] E.M. Golafshani, A. Behnood, M. Arashpour, Predicting the compressive strength of normal and High-Performance Concretes using ANN and ANFIS hybridized with Grey Wolf Optimizer, Constr. Build. Mater. 232 (2020), 117266, https://doi.org/10.1016/j.conbuildmat.2019.117266.
[49] M.A. Khan, F. Aslam, M.F. Javed, H. Alabduljabbar, A.F. Deifalla, New prediction models for the compressive strength and dry-thermal conductivity of bio-composites using novel machine learning algorithms, J. Clean. Prod. 350 (2022), 131364, https://doi.org/10.1016/j.jclepro.2022.131364.
[50] Z. Pei, Y. Wei, Prediction of the bond strength of FRP-to-concrete under direct tension by ACO-based ANFIS approach, Compos. Struct. 282 (2022), 115070, https://doi.org/10.1016/j.compstruct.2021.115070.
[51] M.I. Waris, V. Plevris, J. Mir, N. Chairman, A. Ahmad, An alternative approach for measuring the mechanical properties of hybrid concrete through image processing and machine learning, Constr. Build. Mater. 328 (2022), 126899, https://doi.org/10.1016/j.conbuildmat.2022.126899.
[52] T.J. Ross, Fuzzy Logic with Engineering Applications, 3rd Edition,, John Wiley and Sons Ltd, 2010.
[53] P.B. Sakthivel, A. Ravichandran, N. Alagumurthi, Modelling and prediction of flexural strength of hybrid mesh and fiber reinforced cement-based composites using Artificial Neural Network (YSA), International Journal of GEOMATE (Geotechnique, Construction Materials, and Environment) 10 (1) (2016) 1623–1635. https://geomatejournal.com/geomate/article/view/1993.
[54] G., Ozcan, Y. Kocak, & E. Gulbandilar,, Compressive strength estimation of concrete containing zeolite and diatomite: an expert system implementation, Comput. Concr. 21 (1) (2018) 21–30, https://doi.org/10.12989/cac.2018.21.1.021.
[55] F. Gkountakou, B. Papadopoulos, The use of fuzzy linear regression and ANFIS methods to predict the compressive strength of cement, Symmetry 12 (8) (2020) 1295, https://doi.org/10.3390/sym12081295.
[56] P. Gupta, N. Gupta, K.K. Saxena, S. Goyal, Multilayer perceptron modelling of geopolymer composite incorporating fly ash and GGBS for prediction of compressive strength, Advances in Materials and Processing Technologies 8 (sup3) (2022) 1441–1455, https://doi.org/10.1080/2374068X.2021.1946751.
[57] M. Bilgehan, A comparative study for the concrete compressive strength estimation using neural network and neuro-fuzzy modelling approaches, Nondestructive Testing and Evaluation 26 (01) (2011) 35–55, https://doi.org/10.1080/10589751003770100.
[58] H.S.J. Al-Haidari, I.S. Al-Haydari, Artificial intelligence-based compressive strength prediction of medium to high strength concrete, Iranian Journal of Science and Technology, Transactions of Civil Engineering 46 (2) (2022) 951–964, https://doi.org/10.1007/s40996-021-00717-5.
[59] T.T. Nguyen, H. Pham Duy, T. Pham Thanh, H.H. Vu, Compressive strength evaluation of fiber-reinforced high-strength self-compacting concrete with artificial intelligence, Advances in Civil Engineering 2020 (2020) 1–12, https://doi.org/10.1155/2020/3012139.
[60] D.V. Dao, H.B. Ly, S.H. Trinh, T.T. Le, B.T. Pham, Artificial intelligence approaches for prediction of compressive strength of geopolymer concrete, Materials 12 (6) (2019) 983, https://doi.org/10.3390/ma12060983.